Two motor neuron synergies, invariant across ankle joint angles, activate the triceps surae during plantarflexion

Jackson Levine[1, 2, 3, *], Simon Avrillon[1, 2, 4, *], Dario Farina[4], François Hug[5, 6], José L. Pons[1, 2, 3]

[1] Legs + Walking Lab, Shirley Ryan AbilityLab, Chicago 60611, IL, USA
[2] Department of Physical Medicine and Rehabilitation, Feinberg School of Medicine, Northwestern University, Chicago 60611, IL, USA.
[3] Department of Biomedical Engineering, McCormick School of Engineering, Northwestern University, Chicago 60611, IL, USA.
[4] Department of Bioengineering, Faculty of Engineering, Imperial College London, London W12 7TA, UK
[5] Université Côte d'Azur, LAMHESS, Nice 06200, France
[6] The University of Queensland, School of Biomedical Sciences, St Lucia QLD 4072, QLD, Australia

* These authors equally contributed to this work.

Short title: Invariance of common inputs to motor neurons

Correspondence:
Simon Avrillon
Imperial College London, London, UK
e-mail: s.avrillon@imperial.ac.uk
José L. Pons
Legs + Walking Lab, floor 23
Shirley Ryan AbilityLab, Chicago, IL, USA
e-mail: jpons@sralab.org

Number of pages: 34; Number of figures: 6

Conflict of interests:
The authors declare no competing financial interests.
Funding resources.
Dario Farina is supported by the European Research Council Synergy Grant NaturalBionicS (contract #810346), the EPSRC Transformative Healthcare, NISNEM Technology (EP/T020970), and the BBSRC, "Neural Commands for Fast Movements in the Primate Motor System" (NU-003743). François Hug is supported by a fellowship from the French government, through the UCAJEDI Investments in the Future and by the National Research Agency (ANR) with the reference number ANR-15-IDEX-01. Jose L. Pons is supported by the National Science Foundation/National Robotics Initiative under Grant 2024488.

Abstract

Recent studies have suggested that the nervous system generates movements by controlling groups of motor neurons (synergies) that do not always align with muscle anatomy. In this study, we determined whether these synergies are robust across tasks with different mechanical constraints. We identified motor neuron synergies using principal component analysis (PCA) and cross-correlations between smoothed discharge rates of motor neurons. In Part 1, we used simulations to validate these methods. The results suggested that PCA can accurately identify the number of common inputs and their distribution across active motor neurons. Moreover, the results confirmed that cross-correlation can separate pairs of motor neurons that receive common inputs from those that do not receive common inputs. In Part 2, sixteen individuals performed plantarflexion at three ankle angles while we recorded electromyographic signals from the gastrocnemius lateralis (GL) and medialis (GM) and the soleus (SOL) with grids of surface electrodes. PCA revealed two motor neuron synergies. These motor neuron synergies were relatively stable with no significant differences in the distribution of motor neuron weights across ankle angles ($p=0.62$). When the cross-correlation was calculated for pairs of motor units tracked across ankle angles, we observed that only 13.0% of pairs of motor units from GL and GM exhibited significant correlations of their smoothed discharge rates across angles, confirming the low level of common inputs between these muscles. Overall, these results highlight the modularity of movement control at the motor neuron level, suggesting a sensible reduction of computational resources for movement control.

Key points summary:

- The central nervous system may generate movements by activating groups of motor neurons (synergies) with common inputs.
- We show here that two main sources of common inputs drive the motor neurons innervating the triceps surae muscles during isometric ankle plantarflexions.
- We report that the distribution of these common inputs is globally invariant despite changing the mechanical constraints of the tasks, i.e., the ankle angle.
- These results suggest the functional relevance of the modular organization of the central nervous system to control movements.

Introduction

The neural control of movement relies on the coordinated activity of numerous motor units. A large proportion of these motor units receives common synaptic inputs (Laine *et al.*, 2015; Negro *et al.*, 2016b), which arise from various sources, including descending commands and proprioceptive feedback (Heckman & Binder, 1993; Lemon, 2008; Heckman & Enoka, 2012; Laine *et al.*, 2014; Glover & Baker, 2022). Simulation studies have shown that the pool of motor neurons tends to linearly transmit these common synaptic inputs to the muscle while it attenuates independent inputs (Farina *et al.*, 2014b). Thus, the time-varying modulation of muscle force during a sustained isometric contraction mainly depends on the modulation of common synaptic inputs, as evidenced by the significant correlation between the low-pass filtered cumulative spike train of motor units and muscle force (De Luca & Erim, 2002; Negro *et al.*, 2009; Thompson *et al.*, 2018).

When considering the coordination of multiple muscles, common synaptic inputs may also be distributed across groups of motor units that share a similar function to generate a force in a desired direction (Tresch & Jarc, 2009; Bizzi & Cheung, 2013). This distribution outlines a modular organization of low dimensionality, theorized as synergies, or motor modules, and mainly demonstrated at the muscle level by combining the recording of multiple muscles with bipolar electromyography (EMG) and factorization algorithms (Tresch *et al.*, 1999; d'Avella *et al.*, 2003; Ting *et al.*, 2015; Yaron *et al.*, 2020). The recent development of algorithms that discriminate the discharge activity of individual motor units has changed the scale of this approach, with synergies now being considered at the motor neuron level. These motor neuron synergies can group subsets of motor neurons within each muscle or across portions of different muscles (Hug *et al.*, 2023b). For example, it has been shown that motor neurons innervating a single muscle can be separated into several synergies based on their fluctuations of discharge rate, even during tasks of a single degree of freedom (Madarshahian *et al.*, 2021; Del Vecchio *et al.*, 2023).

To date, the identification of motor neuron synergies has only been reported for motor tasks with stable mechanical constraints (Madarshahian *et al.*, 2021; Del Vecchio *et al.*, 2023; Hug *et al.*, 2023b). It remains unknown whether the distribution of common inputs to groups of motor neurons is robust across motor tasks, as observed for muscle synergies (d'Avella *et al.*, 2003). Addressing this question is fundamental to prove that the observed motor neuron synergies feature an effective

way of simplifying the neural control of movement through motor modules that are invariant across a repertoire of tasks.

The technical challenge of identifying motor neuron synergies across tasks is that motor neurons must be tracked across contractions. However, EMG decomposition is currently only applicable during isometric contractions with slight changes in muscle length (Farina & Holobar, 2016). Indeed, this procedure relies on the stability of muscle geometry to identify consistent spatiotemporal profiles of motor unit action potentials with the grid of surface electrodes (Martinez-Valdes *et al.*, 2017; Del Vecchio & Farina, 2019; Oliveira & Negro, 2021). For this reason, we identified in this study motor neurons innervating the triceps surae muscles (soleus [SOL], gastrocnemius medialis [GM], and gastrocnemius lateralis [GL]) and tracked them during isometric contractions performed at three different ankle angles. These muscles are interesting as an uncoupling of their neural drives has been demonstrated during sustained contractions (Hug *et al.*, 2021b; Rossato *et al.*, 2022), despite all being connected to the same distal tendon and being grouped within the same muscle synergy during most natural behaviors. Similarly, it was shown that changes in neural drive, due to the alteration of force generating capacity during an ankle rotation, may differ between GL and GM/SOL (Lacourpaille *et al.*, 2017). This suggests that the central nervous system may control several motor modules, even during a task with a single degree of freedom (Lacourpaille *et al.*, 2017; Rossato *et al.*, 2022).

In this study, we identified motor neuron synergies by estimating the distribution of common synaptic inputs to groups of motor neurons innervating the triceps surae muscles. To this end, we used principal component analysis and cross-correlation of their smoothed discharge rates (Fig. 1A). To validate our approach, we first simulated 100 motor neurons receiving two sources of common synaptic input, and we assessed whether the proposed methods could identify the low dimensional control of motor neuron behavior. Then, we recorded EMG signals from the triceps surae muscles in sixteen participants to evaluate the robustness of motor neuron synergies across tasks. We hypothesized that 1) despite the single dimension captured by the classic EMG analysis at the muscle level (e.g., van den Hoorn *et al.*, 2015), the dimensionality of control would be greater than one at the motor neuron level, and 2) the structure of the motor neuron synergies would remain invariant across joint angles. The validation of these hypotheses would prove that the central nervous system controls movements by distributing common inputs to stable groups of motor neurons, ensuring a sensible reduction of dimensions for movement control.

Methods

Part 1: Simulations

We first aimed to test the sensitivity of our methods to capture the low dimensional control of motor neurons (Fig. 1B). As previous studies have shown different changes in neural drive between GL and GM/SOL during constrained isometric plantarflexions (Lacourpaille *et al.*, 2017; Hug *et al.*, 2021b), we hypothesized that two main sources of common inputs may drive the triceps surae muscles during plantarflexion. Thus, we simulated 100 motor neurons receiving common and independent synaptic inputs with the model developed by Elias and Kohn (2013), with one compartment for the soma and one compartment for the dendritic tree. This model is an updated version of a previously published motor neuron model (Cisi & Kohn, 2008), with the addition of a L-type Ca^{++} channel into the dendritic compartment to consider the non-linearity between motor neuron inputs and outputs due to persistent inward currents (Heckman & Enoka, 2012). Geometric and electronic parameters of the 100 motor neurons were linearly interpolated from the range of values reported in Table 1 of Elias and Kohn (2013) for a S-type motor unit.

The total synaptic input for each motor neuron was the linear summation of common and independent inputs simulated as white Gaussian noise. The common and independent inputs had equal variances, with a bandwidth of 0-2.5Hz for the common inputs, and a bandwidth of 0-50Hz for the independent inputs. The mean and the variance of the total synaptic input were tuned to generate physiologically realistic distributions of interspike intervals (Negro *et al.*, 2016b). To simulate motor neuron synergies, we generated two uncorrelated sources of common synaptic inputs with a range of synaptic weights for the pool of motor neurons. Specifically, 20 motor neurons received 100% of common input (CI) #1, 20 motor neurons received 100% of CI#2, and 60 motor neurons received CI#1 and CI#2 with synaptic weights ranging from 99% CI#1/1% CI#2 to 1% CI#1/99% CI#2. The synaptic weights were shuffled across the 100 motor neurons and fixed for all the simulations.

We generated three simulations with different amplitudes of the two common inputs. In the first simulation, the amplitude of common inputs #1 and #2 were equal (CI#1 = CI#2). In the second (CI#1+ CI#2) and third simulations (CI#1++ CI#2), the amplitude of common input #1 was amplified to generate an averaged increase in discharge rate of 1 pps between each condition for all the motor neurons receiving this input (Fig. 1B). This idea was to mimic the divergent

modulation of two separate sources of common synaptic inputs and to match the discharge rates experimentally observed during the plantarflexions.

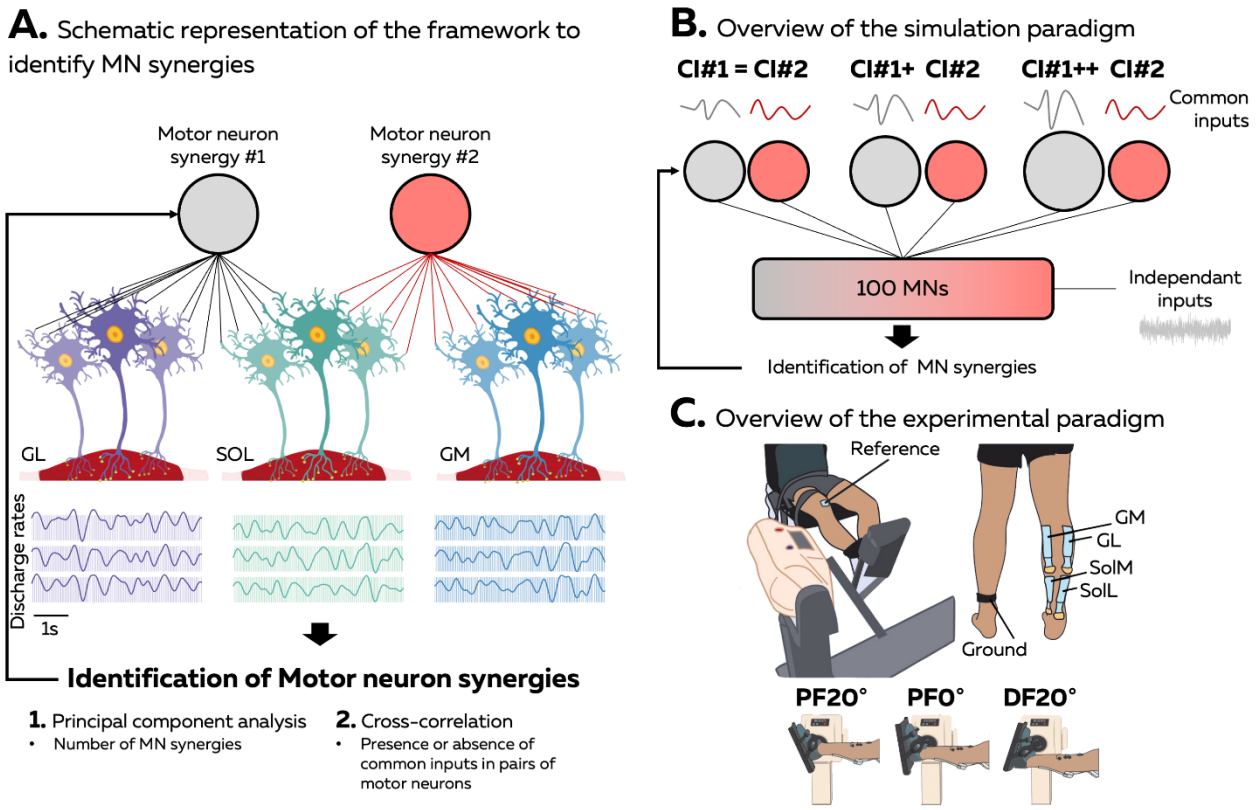

Figure 1: Overview of the study. We aimed to identify motor neuron synergies driving the triceps surae muscles during ankle plantarflexion. (A) We hypothesized that two motor neuron synergies would drive the gastrocnemius lateralis (GL), soleus (SOL), and gastrocnemius medialis (GM) muscles. To test this hypothesis, we needed to identify the distribution of common inputs to the pool of motor neurons. Thus, we applied principal component analyses (PCA) and cross-correlation on motor neuron smoothed discharge rates. (B) We first assessed the ability of these methods to identify the distribution of common inputs across motor neurons using 100 simulated motor neurons driven by two sources of common inputs with known synaptic weights. We changed the amplitude of these inputs to mimic the divergent variations in discharge rate observed experimentally between GL and GM/SOL muscles. (C) Then, we identified and tracked motor units from electromyographic signals recorded from the GL, GM, and SOL muscles across three ankle angles. As for the simulation, we determined whether the distribution of common inputs to the tracked motor units was robust across the three conditions using PCA and cross-correlation.

Part 2: Experiments

In the second part of the study, we identified and tracked the motor neuron synergies driving the triceps surae muscles during plantarflexions performed at three ankle joint angles (Fig. 1C).

178

179 ***Ethical approval and participants***

180 A sample of sixteen individuals, with an equal number of males (n = 8; age: 28 ± 4 years, height:
181 178 ± 6 cm, body mass: 77 ± 10 kg) and females (n = 8; age: 29 ± 11 years, height: 162 ± 8 cm,
182 body mass: 60 ± 9 kg), volunteered to participate in this experiment. They had no history of
183 knee/ankle injury in the last six months before the experiments nor lower leg pain that would impact
184 their ability to complete the voluntary contractions. The institutional review board (IRB) of
185 Northwestern University reviewed and approved the protocol of this study (STU00212191), which
186 followed the standards of the declaration of Helsinki. Participants provided their informed written
187 consent before starting the experimental session.

188

189 ***Protocol***

190 Participants sat on a dynamometer (Biodex System 4 Pro, Biodex Medical, Shirley, NY) with their
191 hip flexed at 90º (0º being the neutral position) and their knee fully extended (Fig. 1C). The foot of
192 the dominant leg (i.e., right leg for all the participants) was fixed to a pedal that held the ankle at
193 specified angles (Fig. 1C). Two inextensible straps immobilized their torso, while additional straps
194 around the waist and the thigh of the dominant leg ensured that force generation solely relied on
195 the calf muscles.

196 All experimental tasks consisted of isometric ankle plantarflexion. The participants first performed
197 a standardized warm-up with their ankle positioned at neutral position (0º, i.e., the foot is
198 perpendicular to the shank). Participants were asked to push against the pedal with gradually
199 increasing effort, beginning at about 50% of their subjective maximum capabilities. After three
200 contractions, participants were asked to increase effort until they reached about 80-90% of their
201 subjective maximum capabilities.

202 After the warm-up, experimentation began. The experimental protocol was repeated for three
203 different conditions in a randomized order: the ankle plantarflexed at 20º (PF20°), at 0º (PF0°), and
204 dorsiflexed at 20º (DF20°) (Fig. 1C). For each condition, participants performed two maximal
205 isometric voluntary contractions (MVC) for 3-5 s, with 60 s of rest in between. The peak torque
206 was calculated using a moving average window of 250 ms, and the maximal value was used to set
207 the target of the submaximal isometric contractions at 20% of the MVC. After 60 s of rest,
208 participants performed three trapezoidal contractions, consisting of a 15 s linear ramp-up, 30 s

plateau at 20% of the MVC, and 15 s linear ramp-down. These three trapezoidal contractions were separated by 10 s of rest. Target and torque output feedback were displayed on a monitor in front of the participants. The EMG acquisition system (EMG-Quattrocento; 400-channel EMG amplifier, OT Bioelettronica, Italy) was used to digitize the torque signal at a sampling rate of 2048 Hz. Torque signals were low pass filtered (3rd order Butterworth filter, cutoff frequency: 20 Hz) and baseline corrected to remove the weight of the leg and the pedal. The torque accuracy was calculated as the root mean squared error (RMSE) of the signal over the plateau.

EMG recording

Surface EMG signals were recorded from the gastrocnemius medialis (GM), gastrocnemius lateralis (GL), and the lateral and medial regions of the soleus (SOL) using two-dimensional adhesive grids of 64 electrodes (GR08MM1305, 13x5 gold-coated electrodes with one electrode absent on a corner; interelectrode distance: 8mm, OT Bioelettronica, Italy). The grids were aligned in the fascicle direction for the GM and GL. The grids over the soleus were positioned on each side of the Achilles tendon in the muscle shortening direction. Before placing the electrodes, the skin was shaved and cleaned with an abrasive pad and an alcohol wipe. A semi-disposable biadhesive foam layer was used to hold the grids of electrodes to the skin, and conductive paste filled the cavities of the adhesive layers to make skin-electrode contact. Reference electrodes (Ag/AgCl snap electrodes, Noraxon, USA) were placed over the tibia. The EMG signals were recorded in monopolar mode, bandpass filtered at 10-500 Hz, and digitized at a sampling rate of 2048 Hz using the multichannel EMG acquisition system (EMG-Quattrocento, 400 channel EMG amplifier; OT Bioelettronica, Italy).

Data Analysis

Data were analyzed using MATLAB custom-written scripts (R2021a; The MathWorks, Natick, MA).

EMG decomposition

The monopolar EMG signals were bandpass filtered between 20 and 500 Hz with a second-order Butterworth filter. After visual inspection, channels with low signal-to-noise ratio or artifacts were

discarded. The EMG signals were then decomposed into motor unit pulse trains with a blind-source separation algorithm (Negro *et al.*, 2016a). In short, the EMG signals were first extended and whitened. Thereafter, a fixed-point algorithm optimized filters that maximize the level of sparsity of the identified sources of the EMG signal, i.e., the motor unit pulse trains. The high peaks of the motor unit pulse trains were considered as discharge times and separated from the noise using K-means classification. A second algorithm refined the estimation of the discharge times by minimizing the coefficient of variation of the inter-spike intervals while iteratively optimizing motor unit filters. This decomposition procedure has been validated using experimental and simulated signals (Negro *et al.*, 2016a). After the automatic identification of the motor units, all the motor unit pulse trains were visually inspected. The automatic detection of discharge times was manually edited for false positives and false negatives when necessary (Del Vecchio *et al.*, 2020; Hug *et al.*, 2021a). Motor units with a pulse-to-noise ratio above 30 dB after manual editing were retained for further analysis (Holobar *et al.*, 2014).

Crosstalk and duplicates between motor units

We carefully checked all identified motor units for potential crosstalk or duplicates between the two SOL locations, thus ensuring the uniqueness of each motor unit within the dataset (Hug *et al.*, 2021b). To this end, we used the discharge times as triggers to segment the EMG signals differentiated in the column direction for each grid and identify the motor unit action potentials' profiles. Then, we calculated the average peak-to-peak amplitude of the action potentials for all grids. We considered that a motor unit was falsely associated with a muscle due to crosstalk when the peak-to-peak amplitude was larger in a neighboring muscle than in the muscle of origin. On average, 2.6 ± 2.5 MUs were discarded from the analysis per participant. In addition, we verified that no motor units were identified from both grids located over the lateral and the medial parts of the SOL. We considered motor units as duplicates when they shared at least 30% of their discharge times with a tolerance of one data point (i.e., 0.5 ms; (Holobar *et al.*, 2014)). At the end of these analyses, motor units identified over the lateral and medial parts of the SOL were pooled, with on average 0.7 ± 1.4 MUs discarded per participant.

Motor unit tracking

To assess whether a change in muscle length impacts the distribution of common synaptic inputs and motor unit behavior, we matched motor units across ankle angles. For this, we used the unique spatiotemporal profiles of motor unit action potentials within the grids of electrodes (Martinez-Valdes *et al.*, 2017; Del Vecchio & Farina, 2019; Oliveira & Negro, 2021). EMG signals were first differentiated in the column direction to obtain 59 single-differential EMG signals. We then identified motor unit action potential profiles by spike-triggered averaging each of the 59 EMG signals. As the position of the action potentials within the window may differ between motor units, we considered the local maxima, i.e., the positive peak of the action potential with the highest energy within the grid, as the center of the 50 ms window. Finally, we concatenated the motor unit action potentials from the 59 channels, and we performed a 2D cross-correlation between motor units. Pairs with a correlation coefficient higher than 0.75 were considered as matches (Martinez-Valdes *et al.*, 2017; Del Vecchio & Farina, 2019). The matches were displayed and visually inspected to guarantee the similarity of motor unit action potentials. Motor units were separately matched between PF20° and PF0° and between DF20° and PF0°. Only motor units matched across the three conditions were considered for the analyses. The average discharge rate was estimated over the torque plateau for all tracked motor units.

Motor neuron synergies

We identified the common dynamics of motor unit smoothed discharge rates in Parts 1 and 2 using principal component analysis (PCA). The motivation behind this analysis was first to assess the ability of PCA to accurately identify the number of common inputs, and then to estimate the relative distribution of these common inputs, or motor neuron synergies, across motor neurons. All motor neurons discharge activities were converted into binary vectors with discharge times equal to one. These binary vectors were then convoluted with a 400-ms Hanning window, such that the correlation was calculated from the oscillations of the discharge rate related to the fluctuation of force (De Luca & Erim, 2002). It is noteworthy that focusing on the lowest bandwidth also limits the effect of the nonlinear relationship between the synaptic input and the output signal (Negro & Farina, 2012). These signals were high pass filtered to remove offsets and trends using a Butterworth filter 2nd order with a cut-off frequency of 0.75 Hz. Finally, we normalized the

smoothed discharge rates between 0 and 1 to avoid any bias of the principal component analysis output related to differences in discharge rates between motor neurons and ankle angles.

Normalized smoothed discharge rates were then concatenated in a n × T matrix, where n is the number of matched motor neurons and T the number of time samples. We applied PCA to this matrix and identified n components ranked with the level of variance explained by each component. To select the number of components of interest (i.e., motor neuron synergies), we fitted portions of the curve of the variance explained with straight lines by iteratively decreasing the number of points considered in the analysis. The number of components of interest was considered as the first data point where the mean squared error of the fit falls under $5e^{-4}$ (Cheung *et al.*, 2005; d'Avella *et al.*, 2011). In our study, this threshold was reached with two components for both the simulated and experimental data. Then, we displayed two-dimensional biplots where x and y coordinates were the weights of each motor neuron in the two first components, and we calculated the angle between vectors. We considered that the higher the angle between two vectors, i.e., two motor neurons, the lower the proportion of inputs shared between these motor neurons. Therefore, we described the changes in the distribution of common synaptic inputs to motor neurons by comparing the angles between conditions.

Pairs of motor neurons receiving common synaptic inputs

For both Part 1 and Part 2, we estimated for each pair of motor neurons whether they received a significant level of common synaptic input. To this end, we calculated the cross-correlation between their smoothed discharge rates over a 10 s window that maximized the number of motor neurons continuously firing during the plateaus of the submaximal contractions. The presence of common synaptic input for each pair of motor neurons was estimated through the maximal cross-correlation coefficient with a maximal lag of ± 100 ms (De Luca & Erim, 2002). We considered that a pair of motor neurons received common synaptic input when the cross-correlation coefficient was statistically significant (Rodriguez-Falces *et al.*, 2017). Specifically, we defined a significance threshold as the 99th percentile of the cross-correlation coefficient distribution generated with resampled versions of all series of discharge times per participant and condition. To this end, we generated random series of discharge times for each motor neuron by bootstrapping the interspike intervals (random sampling with replacement). This random series of discharge times had the same

329 number of discharge times and the same discharge rate (mean and standard deviation) as the
330 original series of discharge times. We repeated this step four times per pair of motor neurons.

331

332 **Statistics**

333 All statistical analyses were performed with RStudio (USA). First, quantile-quantile plots and
334 histograms were displayed to check the normality of the data distribution. If the data were
335 determined not to be normal, they were transformed to remove the skew. All statistical analyses
336 were performed using linear mixed effect models implemented in the R package *lmerTest* with the
337 Kenward-Roger method to estimate the denominator degrees of freedom and the *p*-values. This
338 method considers the dependence of data points (i.e., individual motor neurons) within each
339 participant due to, e.g., common synaptic inputs. When necessary, multiple comparisons were
340 performed using the R package *emmeans*, which adjusts the *p*-value using the Tukey method. The
341 significance level was set at 0.05. Values are reported as mean ± standard deviation.

342 In Part 1, we assessed the ability of our methods to identify the number of synergies and classify
343 the motor neurons according to the weights of the common inputs they receive. After verifying that
344 the PCA accurately predicts the number of motor neuron synergies, we assessed the correlation
345 between the angles calculated between vectors from the biplots and the level of common inputs.
346 Then, we measured the level of common inputs between motor neurons having significant and non-
347 significant cross correlation coefficients between their smoothed discharge rates across
348 simulations. In this way, we aimed to quantify the minimal level of common input needed to reach
349 the level of significance in the three conditions, and assess the maximal level of common input, if
350 any, needed to have non-significant correlations in the three conditions.

351 In Part 2, we first compared MVC and torque RMSE using a linear mixed effects model with
352 Condition (PF20°, PF0°, DF20°) as a fixed effect and Participant as a random effect. The averaged
353 discharge rates of matched motor units were compared using a linear mixed effects model with
354 Condition (PF20°, PF0°, DF20°) and Muscle (GL, GM, SOL) as fixed effects and Participant as a
355 random effect.

356 Then, we used PCA to report the number of motor neuron synergies at each ankle angle for each
357 participant. We calculated the angles between all the motor neurons, and we used a linear mixed
358 effects model to compare these angles with Muscle (GL, GM, SOL, GL-GM, GL-SOL, GM-SOL)

and Condition (PF20°, PF0°, DF20°) as fixed effects and Participant as a random effect. Finally, we assessed the level of common synaptic input to pairs of motor neurons from the same and different muscles using the cross-correlation coefficients between smoothed discharge rates. We used a linear mixed effects model to compare correlation coefficients with Muscle (GL, GM, SOL, GL-GM, GL-SOL, GM-SOL) and Condition (PF20°, PF0°, DF20°) as fixed effects and Participant as a random effect. The ratio of pairs of motor neurons with correlation coefficients above the significance threshold at each ankle angle, as well as the ratio of pairs of motor neurons with significant or non-significant correlations across all angles were also reported.

Results

Part 1: Simulations

We first investigated the ability of our approach to capture the low dimensional control of motor neurons with PCA. The cumulative sum of the variance explained reached a plateau with two components for all simulations (Fig. 2D). The value of variance explained with two components was 68.8, 70.9, and 72.1% for conditions CI#1 = CI#2, CI#1+ CI#2, and CI#1++ CI#2, respectively. The angles between motor neurons ranged between 0° and 135° across the three conditions (Fig. 2F). We computed correlations between the angles and the difference in ratio of common inputs, calculated as the differences in weights of CI#1 between the two motor neurons. For example, two motor neurons receiving 100% CI#1 / 0% CI#2 and 0% CI#1 / 100% CI#2 have a difference in ratio equal to 1. Adjusted R^2 values reached 0.91, 0.91, and 0.92 for conditions CI#1 = CI#2, CI#1+ CI#2, and CI#1++ CI#2, respectively. It demonstrates that the angle between two motor neurons in the biplots is largely explained by the ratio of common inputs they receive, i.e., the greater the angle, the higher the difference in ratio of common inputs (Fig. 2F).

We then performed cross-correlation between smoothed discharge rates of individual motor neurons with a significance threshold fixed at 0.29 (Fig. 2E). Correlation coefficients are displayed in Figure 2E according to the difference in ratio of common inputs. Motor neurons with a difference in ratio of common inputs of 0.29 ± 0.23, 0.30 ± 0.23, and 0.30 ± 0.23 had a significant correlation between their smoothed discharge rates in conditions CI#1 = CI#2, CI#1+ CI#2, and CI#1++ CI#2, respectively. Conversely, motor neurons with a difference in ratio of common inputs of 0.88 ± 0.13, had non-significant correlation between their smoothed discharge rates, and this regardless the condition (Fig. 2E). While 68.5% of the pairs of motor neurons exhibited significant correlations between their smoothed discharge rates across the three simulations, only 20.1% of the pairs exhibited non-significant correlations. These pairs of motor neurons with consistent non-significant correlations across simulations mostly received different inputs, with a difference in ratio of common inputs of 0.93 ± 0.09 (Fig. 2G). Pairs of motor neurons with consistent significant correlations across simulations mostly received the same inputs, with a difference in ratio of common inputs of 0.27 ± 0.21 (Fig. 2G). 11.4% of the pairs of motor neurons had changes in significance across simulated conditions, with differences in ratio of common inputs of 0.71 ± 0.12 (Fig. 2G). It showed that changes in level of correlation in the cross-correlation analysis can be

explained by the amplification of one of the common synaptic inputs, despite fixed ratios of common inputs between simulations. It is noteworthy that it affected a minor proportion of pairs of motor neurons (11.5%) and that motor neurons receiving low or high proportions of the same common inputs had the same level of correlation between the simulations.

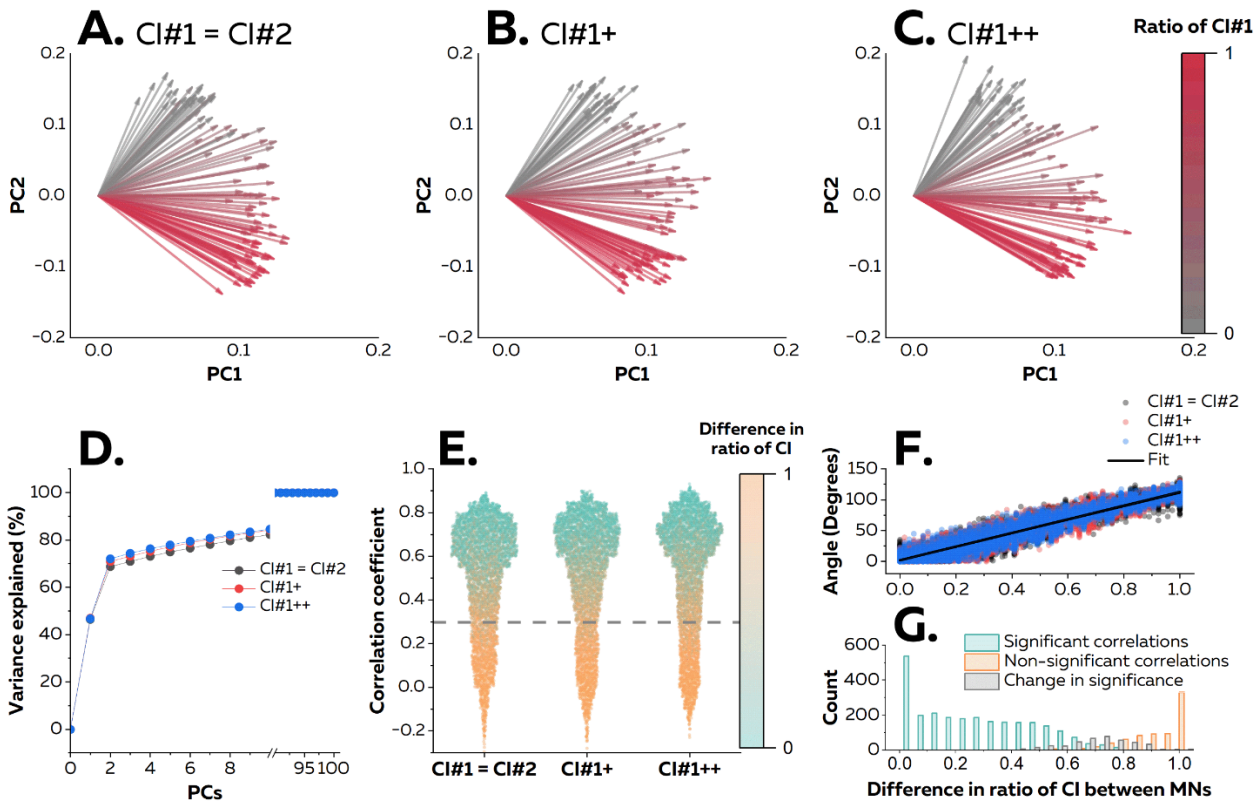

Figure 2: Simulation of a pool of motor neurons with two sources of common synaptic inputs. We simulated 100 motor neurons using an open-source model (Elias & Kohn, 2013). Each motor neuron received either 100% Common input #1 (CI#1, 20 motor neurons), 100% Common input #2 (CI#2, 20 motor neurons), or a ratio of CI#1 and CI#2 from 99% CI#1/ 1% CI#2 to 1% CI#1/ 99% CI#2 (60 motor neurons). We generated three simulations with different amplitudes of the common input #1 to mimic the divergent modulation of two separate sources of common synaptic inputs and to match the discharge rates experimentally observed during the plantarflexions. (A, B, C) We applied principal component analysis (PCA) and displayed the two-dimensional biplots based on the two main components. (D) Indeed, the cumulative sum of the variance explained reached a plateau with two components. Each vector represents an individual motor neuron with the color depending on the ratio of CI#1 received by the motor neuron. (E) Then, we estimated the level of common synaptic input for all pairs of motor neurons using cross-correlation analyses between individual motor neuron smoothed discharge rates. All correlations above 0.29 (dash grey line) were significant. The color of scatters depends on the difference in the ratio of common input #1 between motor neurons in

each pair. For example, two motor neurons receiving 100% CI#1 / 0% CI#2 and 0% CI#1 / 100% CI#2 have a difference in ratio equal to 1. (F) Angles between motor neurons were largely explained by differences in ratio of CI#1. (G) When we modulated the amplitude of CI#1 and CI#2 across simulated conditions, a portion (albeit small) of the pairs exhibited variable levels of correlation. Distribution of difference in ratio for CI#1 for each pair of motor neurons with significant, non-significant, or different level of significance across simulations.

Part 2: Experiments

Torque

As expected, the MVC torque was significantly different between conditions ($F = 36.94$, $p < 0.001$), with MVC torque at PF20° (383.4 ± 225.4 N.m) being significantly lower than that at PF0° (715.7 ± 354.8 N.m, $p < 0.001$) and DF20° (790.0 ± 448.2 N.m, $p < 0.001$). There was no difference between PF0° and DF20° ($p = 0.892$). The RMSE was not significantly different between conditions ($F = 2.73$, $p = 0.082$), meaning that the target torque was matched with similar accuracy across conditions.

Motor unit discharge characteristics

A total of 595 (37 ± 22 per participant; range: 5-79), 613 (38 ± 27 per participant; range: 3-96), and 471 (29 ± 22 per participant; range: 3-76) motor units were identified at PF20°, PF0°, and DF20°, respectively. They had an average pulse-to-noise ratio of 33.3 ± 2.6 dB. 96 motor units (17.2%) were matched over the three conditions, with 17, 45, and 34 motor units for the GL, GM, and SOL, respectively. It is noteworthy that six participants were excluded from the analyses, as no motor units could be matched across conditions, and thus data in this section are reported for the 10 remaining participants. We first compared the discharge characteristics of these tracked motor units (Fig. 3). When considering the average discharge rates, significant effects of Condition ($F = 18.89$, $p < 0.001$), Muscle ($F = 3.41$, $p = 0.034$), and an interaction Condition × Muscle ($F = 2.56$, $p = 0.039$) were observed. The average discharge rate of motor units from the GL was significantly lower at DF20° (8.1 ± 1.8 pps) than at PF20° (10.5 ± 2.5 pps). Similarly, the average discharge rate of motor units from the SOL was significantly lower at DF20° (7.8 ± 2.3 pps) than at PF20° (9.1 ± 2.7 pps). No significant differences were observed for other angles or muscles (all $p > 0.109$).

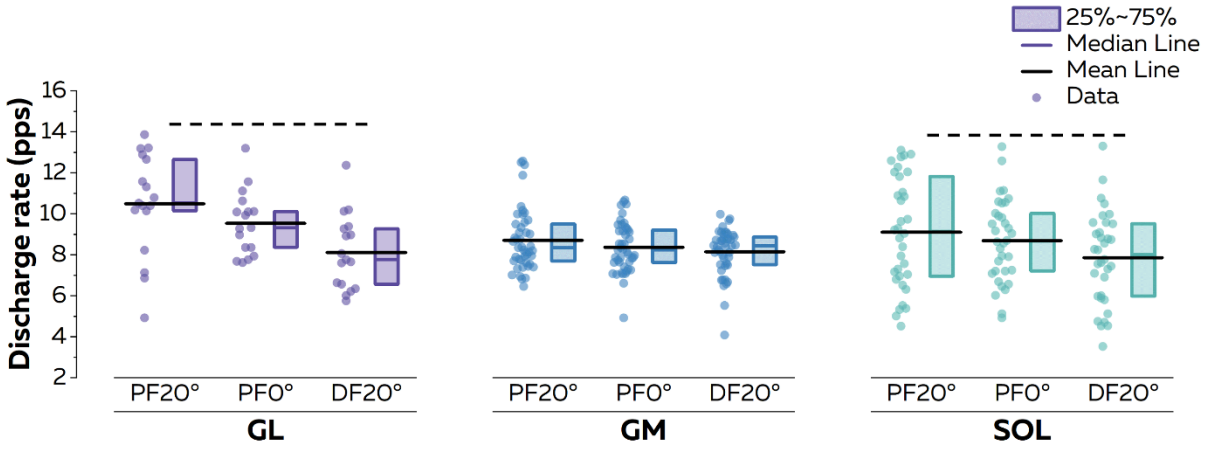

Figure 3: Motor unit discharge rate. We compared the discharge rate of all matched motor units. The average discharge rate was estimated after smoothing instantaneous discharge rates with a 1s Hanning window over the plateau. Each scatter represents an individual motor unit. The horizontal dash lines on top of the plots depict the significant statistical differences with a $p < 0.05$. For the sake of clarity, we only reported the differences within muscles. GL: Gastrocnemius lateralis; GM: Gastrocnemius medialis; SOL: Soleus. PF, Plantarflexion; DF: Dorsiflexion.

Number of common inputs

The motor neuron synergy analysis was performed for participants with motor units identified from all muscles in the three conditions (n = 12 participants; 34 ± 17 MUs per participant). PCA was performed on the normalized smoothed discharge rates. We first intended to identify the number of common inputs, or motor neuron synergies. To this end, we used mean-square error to determine the number of components where the cumulative sum of the variance explained reached a plateau (Cheung *et al.*, 2005; d'Avella *et al.*, 2011). We found on average two motor neuron synergies for the three conditions. The two-dimensional biplots with the weight of each motor neuron in the two motor neuron synergies are displayed in Fig. 4.

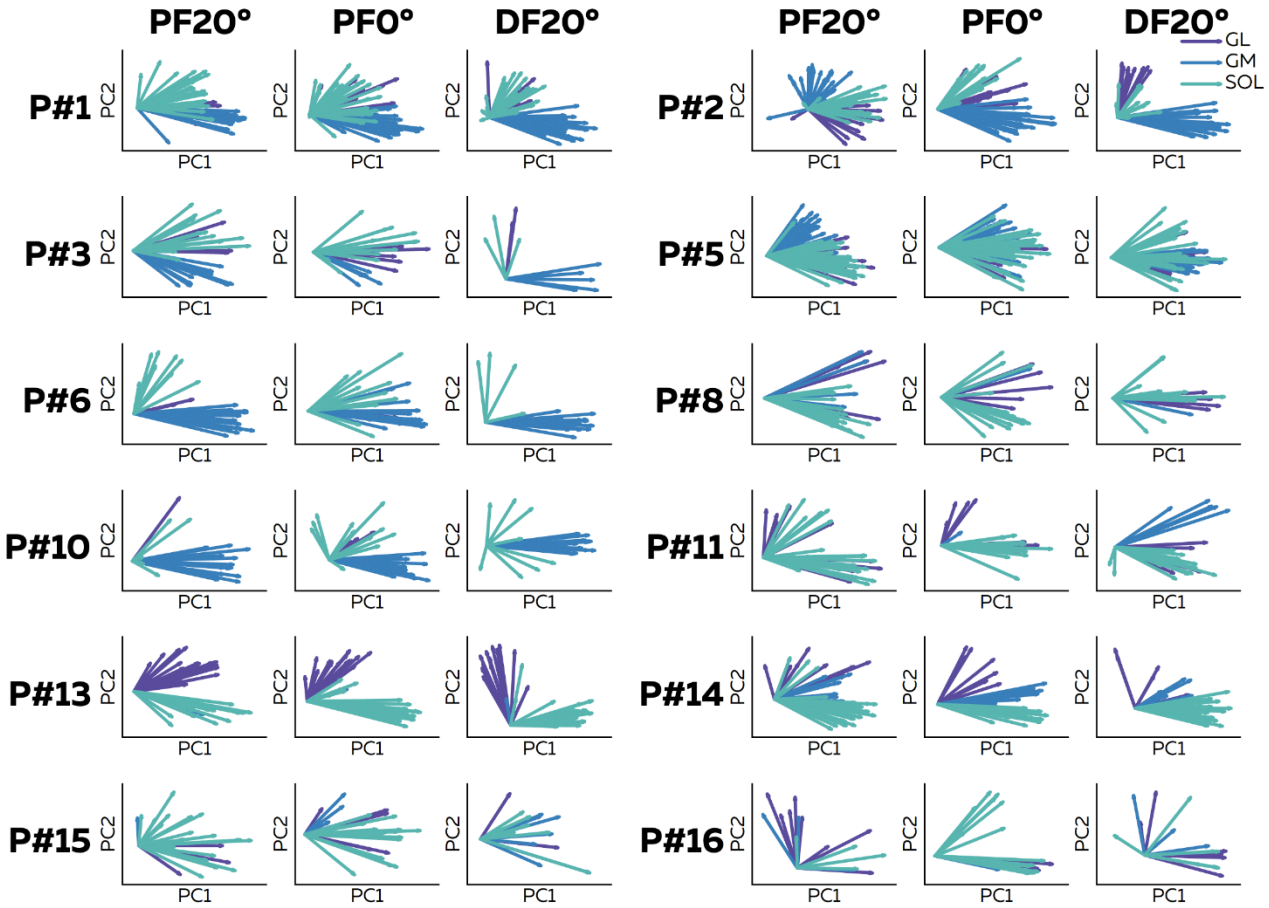

Figure 4: Biplots of motor unit weights from the two motor neuron synergies. For each participant (n=12), we applied principal component analysis on normalized smoothed discharge rates concatenated in a matrix. The identified components were ranked based on the variance they explained, with two components sufficient such that the variance explained reached a plateau. Then, we displayed two dimensional biplots where coordinates of each motor neuron are the weights of the two motor neuron synergies. Each vector represents an individual motor motor neuron. The color of the vector depends on the muscle. GL: Gastrocnemius lateralis; GM: Gastrocnemius medialis; SOL: Soleus.

We then calculated the angles for each pair of vectors (i.e., each pair of motor neurons, n= 26589) in the biplot. Simulations demonstrated that these angles provide a good estimate of the difference in ratio of common inputs between two motor neurons (Fig. 2F). For each of the 12 participants, a mean angle was calculated for each muscle and condition (Fig. 5B). We found a significant main effect of Muscle ($F = 22.28$; $p < 0.001$), but neither a significant main effect of Condition ($F = 0.47$; $p = 0.62$) nor a significant interaction ($F = 1.30$; $p = 0.23$). Specifically, angles were significantly lower between motor neurons within the GL (33.0 ± 22.3°; $p = 0.005$) and within the

GM (23.6 ± 18.2°; $p < 0.001$) than between pairs of motor units within the SOL (50.7 ± 26.6°; Fig. 5B). Moreover, the angles between motor neurons within the GL and within the GM were also significantly lower than the angles between motor neurons from different muscles, i.e., GL-GM, GL-SOL, and GM-SOL (all $p < 0.001$; Fig. 5B). Finally, the angles between motor neurons within the SOL were lower than the angles between motor units of GM-SOL (68.7 ± 15.9°; $p = 0.006$). The differences between pairs of muscles are displayed on Figure 5. Taken together, these results suggest that motor units within the GL or within the GM receive the highest proportion of common input.

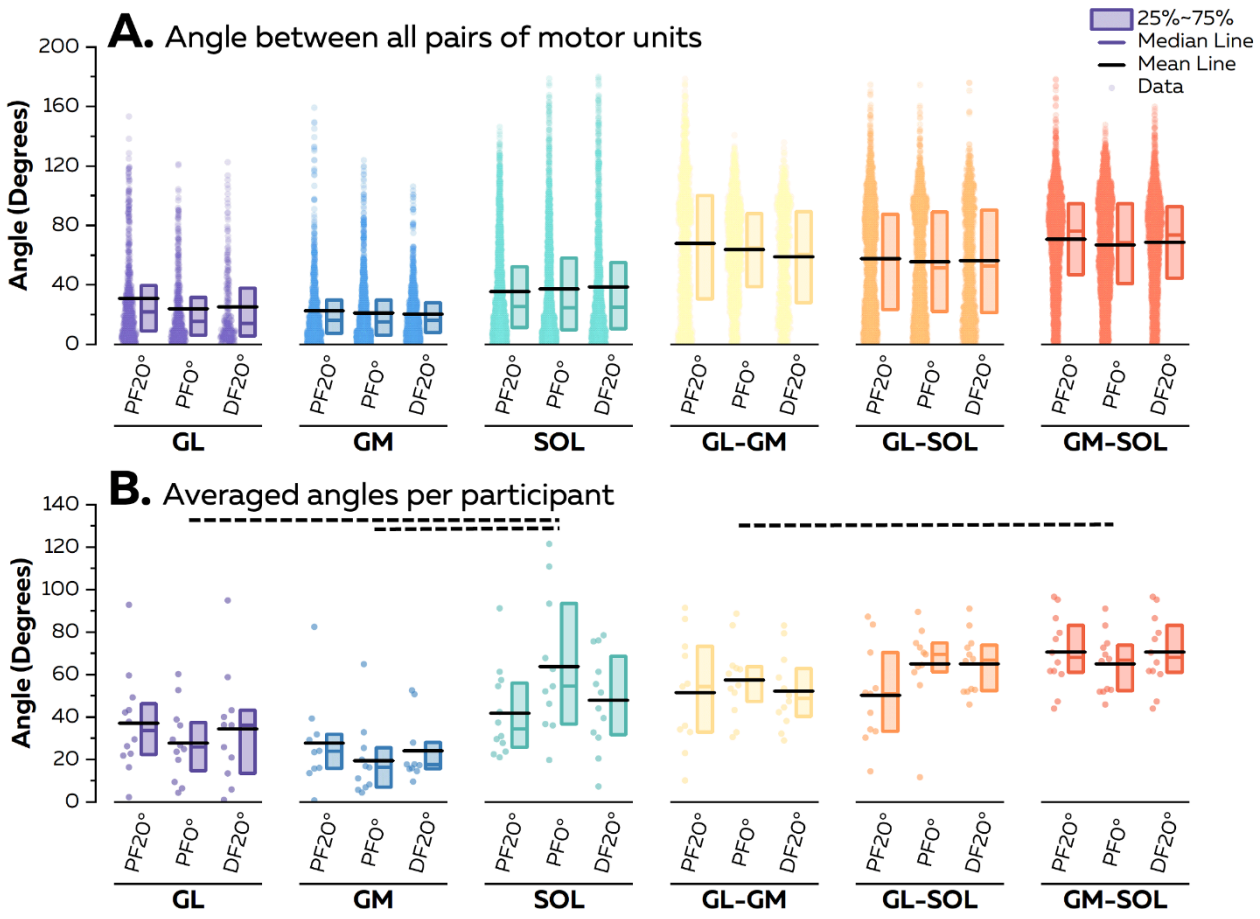

Figure 5: Angles between vectors representing motor neurons in biplots. After applying principal component analysis, we displayed two dimensional biplots where coordinates of each motor neuron were the weights of that motor neuron in each of the two principal components. We then calculated the angles between these vectors to estimate the strength of common inputs received by each pair of motor neurons. (A) We report the angle values for all the pairs of motor neurons. Each scatter represents an individual pair of motor neurons. (B) We then averaged these values per participant and performed the statistical analyses to compare these values between muscles and conditions. Each scatter

represents an individual. The horizontal dash lines on top of the plot depict the significant statistical differences with a $p < 0.05$. For the sake of clarity, note that we did not display the significant difference between GL and GM with all pairs of muscles. GL: Gastrocnemius lateralis; GM: Gastrocnemius medialis; SOL: Soleus; PF, plantarflexion; DF: dorsiflexion.

Distribution of common inputs across motor neurons

We analyzed the correlation for 416 pairs of matched motor units discharge rates. Specifically, we had 34, 147, and 92 pairs of motor neurons for GL, GM, and SOL, respectively, and 46, 29, and 68 pairs of motor neurons for GL-GM, GL-SOL, and GM-SOL, respectively. The coefficients of correlation were significantly different between Conditions ($F = 43.65$, $p < 0.001$) and Muscles ($F = 141.46$, $p < 0.001$) with a significant interaction ($F = 15.14$, $p < 0.001$). Specifically, the coefficients of correlation for pairs of motor neurons within the GL and GM were significantly higher for PF0° ($p < 0.001$) and DF20° ($p < 0.001$) compared to PF20°. The coefficients for the SOL were not significantly different across ankle angles. The coefficients of correlation calculated between motor neurons of GL-GM, GL-SOL and GM-SOL were significantly higher for PF0° than for DF20° ($p = 0.012$, $p < 0.001$, and $p < 0.001$, respectively). The coefficients of correlation calculated between motor neurons of GL-SOL and GM-SOL were also significantly higher for PF0° than for PF20° ($p < 0.001$, and $p < 0.001$, respectively). The ratio of pairs of motor neurons with significant correlations reached on average 98.0%, 96.1%, and 98.2% for GL, GM, and SOL, respectively (Fig. 6B). The ratio of pairs of motor units with significant correlations reached on average 36.9%, 78.2%, and 90.2% for GL-GM, GL-SOL, and GM-SOL, respectively.

We then compared the distribution of common inputs across ankle angles by calculating the ratio of pairs of motor neurons with the same level of correlation (either significant or non-significant correlations) across the three angles (Fig. 6C). The rest of the motor neurons switched between significant and non-significant correlations across ankle angles. None of the pairs of motor neurons had a non-significant level of correlation across all three ankle angles when considering motor neurons from GL, GM, SOL, GL-SOL, and GM-SOL; but 26.1% of pairs of motor neurons from GL-GM had a non-significant level of correlation across all conditions. A high percentage of pairs of motor neurons had a significant level of correlation across all three ankle angles for GL (94.1%), GM (88.4%), and SOL (94.6%) (Fig. 6C). When considering pairs of motor neurons from different muscles, 13.0% (GL-GM), 48.3% (GL-SOL), and 73.5% (GM-SOL) had a consistent significant

level of correlation across angles (Fig. 6C). It is noteworthy that we failed to identify a significant level of correlation in a large percentage of pairs of motor units between GL and GM. Conversely, some pairs of motor neurons from GL-SOL and GM-SOL exhibited significant correlations at all three angles. Together with the absence of significant correlations for most of the GM-GL pairs, it supports the findings from the PCA that two common inputs drive motor neurons innervating the GL, GM, and SOL muscles during ankle plantarflexion.

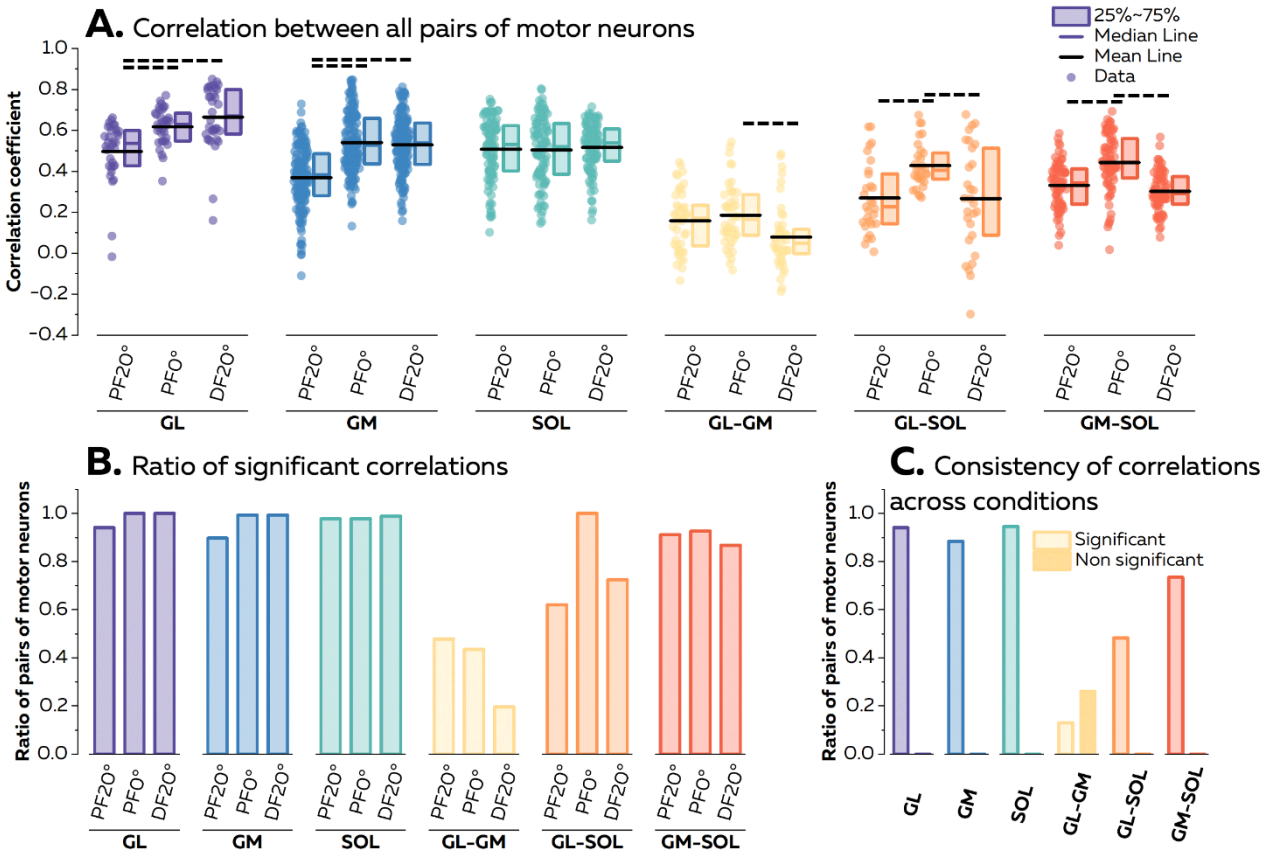

Figure 6: Common inputs to pairs of motor neurons. We estimated the proportion of common synaptic input for all pairs of motor neurons from the same and different muscles using cross-correlation analyses between individual motor neurons smoothed discharge rates. (A) We first compared the level of correlation for each individual muscle and pairs of muscles. Each scatter represents a pair of motor neurons. The horizontal dash lines on top of the plots depict the significant statistical differences with a $p < 0.05$. For the sake of clarity, we only reported the differences for the interaction. (B) We calculated the ratio of pairs of motor neurons with significant correlations for each individual muscle and pairs of muscles. (C) To compare the changes in common synaptic input to pairs of motor neurons across conditions, we calculated the ratio of pairs of motor neurons which exhibited consistent behavior across ankle angles, i.e., either non-significant or significant level of correlation. GL: Gastrocnemius lateralis; GM: Gastrocnemius medialis; SOL: Soleus.

Discussion

This study aimed to test the robustness of motor neuron synergies across isometric plantarflexion tasks performed with different mechanical constraints. In the first part, we used simulated signals to estimate the sensitivity of our methods (i.e., principal component analysis and correlation of smoothed discharge rates) to identify the number of common inputs and their distribution across motor neurons with various weighting. We found that PCA can accurately identify the number of common inputs to groups of motor neurons. Moreover, cross-correlations can accurately identify pairs of motor neurons receiving or not receiving a significant proportion of common inputs. This approach was then applied to experimental data. We identified two main common inputs driving motor neurons innervating the GL, GM, and SOL, with no significant systematic changes in the distribution of weights across ankle angles. These results highlight a modular organization of the control of motor neurons innervating the triceps surae muscles with a reduced dimensionality.

Methodological considerations

Our experiment is a first step toward the demonstration of the modular organization of the neural control of motor neurons across tasks with different mechanical constraints. As previously noted, the assessment of motor neuron synergies across tasks requires the tracking of the same active motor neurons between contractions. To this end, we matched the unique spatiotemporal profiles of the action potentials recorded over the grid of electrodes (Martinez-Valdes *et al.*, 2017; Del Vecchio & Farina, 2019; Oliveira & Negro, 2021). As changes in ankle position inevitably impacted the position and the angle of active muscle fibers relative to the electrodes, the profiles of action potentials slightly varied across conditions. We consequently had a significant reduction in the sample of motor units analyzed across tasks (96 motor units, 17.2% of the total sample). The recent development of intramuscular electrode arrays (Muceli *et al.*, 2022; Chung *et al.*, 2023) may open new perspectives to accomplish this goal of matching motor units across motor tasks as these electrodes may be less affected by the changes in muscle geometry. Additionally, several teams have demonstrated the ability to decompose EMG signals during slow dynamic contractions, which may provide opportunities to show the robustness of motor neuron synergies during more natural behaviors (Glaser & Holobar, 2019; Chen *et al.*, 2020; Oliveira & Negro, 2021).

575 Despite the above-mentioned methodological limitations and perspectives, studying the robustness
576 of the distribution of common inputs driving the triceps surae muscles during plantarflexions
577 performed at multiple angles has revealed relevant results. Previous works highlighted different
578 changes in neural drive between the three muscles of the triceps surae during sustained contractions
579 and in response to the alteration of force generating capacity during an ankle rotation (Lacourpaille
580 *et al.*, 2017; Hug *et al.*, 2021b; Rossato *et al.*, 2022). Additionally, Marshall et al. (2022) have
581 recently shown that the covariation of motor unit discharge rates and their recruitment order may
582 change between short and long muscle lengths. Both results suggested that the central nervous
583 system could drive these muscles with multiple common inputs, even during a task with a single
584 degree of freedom. Our results supported this hypothesis, with the identification of two sources of
585 common inputs driving the triceps surae muscles. Moreover, whether the distribution of common
586 inputs to motor neurons is robust across muscle lengths was unknown. In this study we further
587 described the distribution of the two common inputs within and between muscles, showing a
588 combination of the common inputs across motor neurons.

589

590 **Distribution of common inputs to modulate muscle force**

591 Numerous works have shown that most of the motor neurons from the same muscle display
592 covariations of their discharge rate, which is necessary to modulate force during isometric
593 contractions (Farina *et al.*, 2014b; Farina & Negro, 2015; Enoka & Farina, 2021). These common
594 fluctuations depend on the modulation of common synaptic inputs, received by all motor units
595 (Negro *et al.*, 2009; Farina *et al.*, 2014a; Farina *et al.*, 2014b; Farina & Negro, 2015; Feeney *et al.*,
596 2018). In line with these studies, we observed that none of the 273 pairs of motor units identified
597 within GL, GM or SOL had a non-significant level of correlation for all three ankle angles (Fig.
598 6C). The covariation of discharge rates between motor units from either GL or GM was particularly
599 high, with a ratio of pairs with significant correlation for all three ankle angles reaching 94.1% and
600 88.4% for GL and GM, respectively. This is in agreement with the small angles between vectors
601 identified from the PCA (Fig. 5). Together, these observations indicate that the majority of motor
602 neurons innervating either GL or GM received the two main common inputs with a similar
603 weighting. On the contrary, the degree of covariation of discharge rates between motor neurons
604 from GL and GM was lower than for the other pairs of muscles, with 13% of pairs of motor neurons

605 exhibiting significant correlation across all three ankle angles. This is in agreement with previous
606 work that used methods at the muscle level, such as intermuscular coherence (Hug *et al.*, 2021b;
607 Rossato *et al.*, 2022) or PCA (Mazzo *et al.*, 2022), to assess the covariations of motor unit discharge
608 rates in the triceps surae muscles. Similarly, pairs of motor units from the SOL appear to have
609 lower covariations of discharge rates than from GL and GM. The nervous system may thus take
610 advantage of the geometry and compartmentalization of this muscle (Bolsterlee *et al.*, 2018) to
611 control multiple sources of common input and produce forces in multiple directions (Segal *et al.*,
612 1991; English *et al.*, 1993). Such strategies have been observed in muscles controlling the
613 individual fingers through multiple tendons (Keen & Fuglevand, 2004; Hockensmith *et al.*, 2005;
614 McIsaac & Fuglevand, 2007), or in the biceps brachii producing force for forearm supination and/or
615 elbow flexion (Barry *et al.*, 2009). Alternatively, one may consider the absence of correlation as a
616 result of different non-linear inputs/outputs functions for each motor neuron due to the activation
617 of persistent inward currents (Heckman *et al.*, 2008; Heckman & Enoka, 2012; Binder *et al.*, 2020).
618 However, we focused our analysis on discharge rates oscillations at low frequencies, which are less
619 affected by these non-linear transformations of synaptic inputs (Negro & Farina, 2012; Farina *et*
620 *al.*, 2014b). Therefore, we are confident that the absence of significant correlation identifies motor
621 units receiving the two common inputs with very different weightings, as suggested for motor units
622 from muscles of the upper (Madarshahian *et al.*, 2021; Marshall *et al.*, 2022) and lower limbs (Del
623 Vecchio *et al.*, 2023; Hug *et al.*, 2023b).

624

625 **From muscle to motor neuron synergies**

626 The fact that the central nervous system may group motor units from synergistic muscles to reduce
627 the dimensionality of movement control has been supported for decades by studies identifying
628 muscle synergies (Tresch & Jarc, 2009; Dominici *et al.*, 2011; Bizzi & Cheung, 2013; Ting *et al.*,
629 2015; Takei *et al.*, 2017). Several studies have shown similar levels of correlation between the
630 discharge activities of motor neurons originating from two synergistic muscles as from the same
631 muscle (Del Vecchio *et al.*, 2023; Hug *et al.*, 2023b). Thus, recent studies have proposed to
632 decompose EMG signals to change the scale at which the synergies are described (Madarshahian
633 *et al.*, 2021; Tanzarella *et al.*, 2021; Del Vecchio *et al.*, 2023; Hug *et al.*, 2023a; Hug *et al.*, 2023b).
634 Here, PCA identified two principal components that explained the main variations of discharge

635 rates of the identified motor neurons. It is worth noting that Gibbs et al. (1995) have already
636 reported significant levels of synchronization between the discharge times of motor units from the
637 gastrocnemius and the soleus muscles, consistent with our results outlining the projection of
638 common inputs to the two muscles.

639 The results of this study support three of the hypotheses proposed by Hug *et al.* (2023a) within the
640 motor neuron synergies framework, namely that during movement 1) motor neurons receives
641 common input in relatively large groups; 2) motor neuron synergies may significantly differ from
642 the classical definition of motor neuron pools, such that synergies may span across muscles (i.e.,
643 GL and SOL, GM and SOL) and/or involve only a portion of a muscle (i.e., SOL); and 3) synergies
644 represent motor modules used by the central nervous system to reduce the dimensionality of
645 control. The latter observation is the main novelty of our study. Previous studies identified motor
646 neuron synergies during isometric contractions performed at a single joint angle (Madarshahian *et*
647 *al.*, 2021; Del Vecchio *et al.*, 2023; Hug *et al.*, 2023b) and, therefore, did not demonstrate their
648 invariance across tasks, which is needed to prove a modular organization of movement control
649 (d'Avella *et al.*, 2003; d'Avella & Bizzi, 2005). To this end, we tested the robustness of motor
650 neuron synergies across ankle angles, with no systematic changes in the distribution of principal
651 component weights within and between muscles (Fig. 5), and a large proportion of pairs of motor
652 units consistently having significant and non-significant correlations between their smoothed
653 discharge rates (Fig. 6C). While a minority of pairs of motor units switched between significant
654 and non-significant levels of correlations across ankle angles, our simulation showed that these
655 motor units may receive the two sources of common inputs with relatively balanced weights (i.e.,
656 34%/66% to 49%/51% in the simulation). The different changes in the amplitude of each source of
657 common input may then impact the level of covariation between motor neuron discharge rates
658 across angles. To support this idea, divergent variations in neural drive to the triceps surae muscles
659 have been indirectly observed while the position of the ankle changed during isometric contractions
660 (Huang *et al.*, 2016; Cibulka *et al.*, 2017; Lacourpaille *et al.*, 2017; Hug *et al.*, 2021b). Overall, we
661 suggest that the distribution of common inputs across motor neurons is indeed robust across tasks
662 with some changes in level of correlation due to differential changes in the amplitude of inputs the
663 motor neurons receive.

664 The concept of combining motor neuron synergies to generate movements may bridge the gap
665 between studies supporting modular control and flexible control of motor units. Proponents of

666 flexible control of motor units suggest that motor units from the same muscle may receive
667 independent inputs instead of one common input, explaining changes in recruitment order between
668 the same motor units across multiple tasks (Basmajian, 1963; Formento *et al.*, 2021; Marshall *et*
669 *al.*, 2022). We show here that most of the motor units from the triceps surae muscles may receive
670 two sources of common inputs. The combination of multiple independent inputs may therefore
671 explain why previous works reported changes in recruitment strategies between motor units from
672 the same muscle while changing the mechanical constraints of the task (Desnedt & Gidaux, 1981;
673 ter Haar Romeny *et al.*, 1984; Herrmann & Flanders, 1998; Marshall *et al.*, 2022).

674

675 **Neural structures that shape the modular control of calf muscles**

676 These results suggest that the neural control of movements may be hierarchically organized, where
677 motor modules are controlled instead of individual motor neurons (Loeb *et al.*, 1999). Thus, spinal
678 circuits involving premotor neurons and interneurons may span across motor nuclei to transmit
679 these correlated inputs to synergist muscles (Levine *et al.*, 2014; Takei *et al.*, 2017; Ronzano *et al.*,
680 2021). However, as motor neurons are the final common pathways where inputs from supraspinal
681 centers and afferent fibers converge, we cannot make any inference about the origin of the
682 correlated inputs though several candidates exist. For example, previous works found that the
683 stimulation of the motor cortex (Overduin *et al.*, 2012) or premotor neurons in the spinal cord
684 (Takei *et al.*, 2017) evoked synergies comparable to those observed during natural behaviors.
685 Additionally, Cheung et al. (2005) observed similar synergies in animals with intact and
686 deafferented nervous systems, suggesting that the activation of synergies would mostly be a
687 feedforward process. Alternatively, others proposed that the correlated activity between synergistic
688 muscles may aim to regulate mechanical features such as internal joint stress, thus emphasizing the
689 key role of sensory feedback (Alessandro *et al.*, 2020). This could also be the case in our study as
690 the variation of ankle angles undoubtedly impacts the behavior of motor neurons during
691 plantarflexions (Kennedy & Cresswell, 2001; Trypidakis *et al.*, 2022). Additionally, the two motor
692 modules may allow the central nervous system to tune the behavior of the lateral and medial
693 portions of the calf muscles to stabilize the foot producing plantarflexion in the frontal plane (Lee
694 & Piazza, 2008), thus limiting the strain and the stress of the ankle joint. Overall, future work is

needed to identify the neural bases of common inputs to motor neurons during voluntary movements (Cheung & Seki, 2021).

Conclusion

Our results support the idea that the central nervous system may combine motor modules to produce ankle plantarflexion. Specifically, we identified two motor neuron synergies grouping motor neurons innervating the triceps surae muscles during plantarflexion performed at multiple ankle angles. Importantly, we found that the structure of these motor neuron synergies is mostly invariant across conditions despite the variation of mechanical constraints, with some level of flexibility that may be accounted for by differential changes in the amplitude of each input. This provides a novel observation that contributes to demonstrate the functional relevance of such modular structures to generate movements.

Acknowledgements

We thank Allie Levine for her illustration in Figure 1.

Data Availability Declaration

Data and codes will be made available upon request to the authors.

References

Alessandro C, Barroso FO, Prashara A, Tentler DP, Yeh HY & Tresch MC. (2020). Coordination amongst quadriceps muscles suggests neural regulation of internal joint stresses, not simplification of task performance. *Proc Natl Acad Sci U S A* **117,** 8135-8142.

Barry BK, Pascoe MA, Riek S, Carson RG & Enoka RM. (2009). Common input to different regions of biceps brachii long head. *Exp Brain Res* **193,** 351-359.

Basmajian JV. (1963). Control and training of individual motor units. *Science* **141,** 440-441.

Binder MD, Powers RK & Heckman CJ. (2020). Nonlinear Input-Output Functions of Motoneurons. *Physiology (Bethesda)* **35,** 31-39.

Bizzi E & Cheung VC. (2013). The neural origin of muscle synergies. *Front Comput Neurosci* **7,** 51.

Bolsterlee B, Finni T, D'Souza A, Eguchi J, Clarke EC & Herbert RD. (2018). Three-dimensional architecture of the whole human soleus muscle in vivo. *PeerJ* **6,** e4610.

Chen C, Ma S, Sheng X, Farina D & Zhu X. (2020). Adaptive Real-Time Identification of Motor Unit Discharges From Non-Stationary High-Density Surface Electromyographic Signals. *IEEE Trans Biomed Eng* **67,** 3501-3509.

Cheung VC, d'Avella A, Tresch MC & Bizzi E. (2005). Central and sensory contributions to the activation and organization of muscle synergies during natural motor behaviors. *J Neurosci* **25,** 6419-6434.

Cheung VCK & Seki K. (2021). Approaches to revealing the neural basis of muscle synergies: a review and a critique. *J Neurophysiol* **125,** 1580-1597.

Chung B, Zia M, Thomas K, Michaels JA, Jacob A, Pack A, Williams M, Nagapudi K, Teng LH, Arrambide E, Ouellette L, Oey N, Gibbs R, Anschutz P, Lu J, Wu Y, Kashefi M, Oya T, Kersten R, Mosberger A, O'Connell S, Wang R, Marques H, Mendes AR, Lenschow C, Kondakath G, Kim JJ, Olson W, Quinn K, Perkins P, Gatto G, Thanawalla A, Coltman S, Kim T, Smith T, Binder-Markey B, Zaback M, Thompson CK, Giszter S, Person A, Goulding M, Azim E, Thakor N, O'Connor D, Trimmer B, Lima SQ, Carey M, Pandarinath C, Costa RM, Pruszynski JA, Bakir M & Sober SJ. (2023). Myomatrix arrays for high-definition muscle recording. *bioRxiv*, 2023.2002.2021.529200.

Cibulka M, Wenthe A, Boyle Z, Callier D, Schwerdt A, Jarman D & Strube MJ. (2017). Variation in Medial and Lateral Gastrocnemius Muscle Activity with Foot Position. *International journal of sports physical therapy* **12,** 233-241.

Cisi RR & Kohn AF. (2008). Simulation system of spinal cord motor nuclei and associated nerves and muscles, in a Web-based architecture. *Journal of computational neuroscience* **25,** 520-542.

d'Avella A & Bizzi E. (2005). Shared and specific muscle synergies in natural motor behaviors. *Proc Natl Acad Sci U S A* **102,** 3076-3081.

d'Avella A, Portone A & Lacquaniti F. (2011). Superposition and modulation of muscle synergies for reaching in response to a change in target location. *J Neurophysiol* **106,** 2796-2812.

d'Avella A, Saltiel P & Bizzi E. (2003). Combinations of muscle synergies in the construction of a natural motor behavior. *Nat Neurosci* **6,** 300-308.

De Luca CJ & Erim Z. (2002). Common drive in motor units of a synergistic muscle pair. *J Neurophysiol* **87,** 2200-2204.

Del Vecchio A & Farina D. (2019). Interfacing the neural output of the spinal cord: robust and reliable longitudinal identification of motor neurons in humans. *J Neural Eng* **17,** 016003.

Del Vecchio A, Holobar A, Falla D, Felici F, Enoka RM & Farina D. (2020). Tutorial: Analysis of motor unit discharge characteristics from high-density surface EMG signals. *J Electromyogr Kinesiol* **53,** 102426.

Del Vecchio A, Marconi Germer C, Kinfe TM, Nuccio S, Hug F, Eskofier B, Farina D & Enoka RM. (2023). The Forces Generated by Agonist Muscles during Isometric Contractions Arise from Motor Unit Synergies. *J Neurosci* **43,** 2860-2873.

Desnedt HE & Gidaux E. (1981). Spinal motoneuron recruitment in man: rank deordering with direction but not with speed of voluntary movement. *Science* **214,** 933-936.

Dominici N, Ivanenko YP, Cappellini G, d'Avella A, Mondi V, Cicchese M, Fabiano A, Silei T, Di Paolo A, Giannini C, Poppele RE & Lacquaniti F. (2011). Locomotor primitives in newborn babies and their development. *Science* **334,** 997-999.

Elias LA & Kohn AF. (2013). Individual and collective properties of computationally efficient motoneuron models of types S and F with active dendrites. *Neurocomputing* **99,** 521-533.

English AW, Wolf SL & Segal RL. (1993). Compartmentalization of muscles and their motor nuclei: the partitioning hypothesis. *Physical therapy* **73,** 857-867.

Enoka RM & Farina D. (2021). Force Steadiness: From Motor Units to Voluntary Actions. *Physiology (Bethesda)* **36,** 114-130.

Farina D & Holobar A. (2016). Characterization of Human Motor Units From Surface EMG Decomposition. *Proceedings of the Ieee* **104,** 353-373.

Farina D, Merletti R & Enoka RM. (2014a). The extraction of neural strategies from the surface EMG: an update. *J Appl Physiol (1985)* **117,** 1215-1230.

Farina D & Negro F. (2015). Common synaptic input to motor neurons, motor unit synchronization, and force control. *Exerc Sport Sci Rev* **43,** 23-33.

Farina D, Negro F & Dideriksen JL. (2014b). The effective neural drive to muscles is the common synaptic input to motor neurons. *J Physiol* **592,** 3427-3441.

Feeney DF, Mani D & Enoka RM. (2018). Variability in common synaptic input to motor neurons modulates both force steadiness and pegboard time in young and older adults. *J Physiol* **596,** 3793-3806.

Formento E, Botros P & Carmena JM. (2021). Skilled independent control of individual motor units via a non-invasive neuromuscular-machine interface. *J Neural Eng* **18**.

Gibbs J, Harrison LM & Stephens JA. (1995). Organization of inputs to motoneurone pools in man. *J Physiol* **485 (Pt 1),** 245-256.

Glaser V & Holobar A. (2019). Motor Unit Identification From High-Density Surface Electromyograms in Repeated Dynamic Muscle Contractions. *IEEE Trans Neural Syst Rehabil Eng* **27,** 66-75.

Glover IS & Baker SN. (2022). Both Corticospinal and Reticulospinal Tracts Control Force of Contraction. *J Neurosci* **42,** 3150-3164.

Heckman CJ & Binder MD. (1993). Computer simulations of the effects of different synaptic input systems on motor unit recruitment. *J Neurophysiol* **70,** 1827-1840.

Heckman CJ & Enoka RM. (2012). Motor unit. *Compr Physiol* **2,** 2629-2682.

Heckman CJ, Johnson M, Mottram C & Schuster J. (2008). Persistent inward currents in spinal motoneurons and their influence on human motoneuron firing patterns. *Neuroscientist* **14,** 264-275.

Herrmann U & Flanders M. (1998). Directional tuning of single motor units. *J Neurosci* **18,** 8402-8416.

Hockensmith GB, Lowell SY & Fuglevand AJ. (2005). Common input across motor nuclei mediating precision grip in humans. *J Neurosci* **25,** 4560-4564.

Holobar A, Minetto MA & Farina D. (2014). Accurate identification of motor unit discharge patterns from high-density surface EMG and validation with a novel signal-based performance metric. *J Neural Eng* **11,** 016008.

Huang C, Chen X, Cao S & Zhang X. (2016). Muscle-tendon units localization and activation level analysis based on high-density surface EMG array and NMF algorithm. *J Neural Eng* **13,** 066001.

Hug F, Avrillon S, Del Vecchio A, Casolo A, Ibanez J, Nuccio S, Rossato J, Holobar A & Farina D. (2021a). Analysis of motor unit spike trains estimated from high-density surface electromyography is highly reliable across operators. *J Electromyogr Kinesiol* **58,** 102548.

Hug F, Avrillon S, Ibanez J & Farina D. (2023a). Common synaptic input, synergies and size principle: Control of spinal motor neurons for movement generation. *J Physiol* **601,** 11-20.

Hug F, Avrillon S, Sarcher A, Del Vecchio A & Farina D. (2023b). Correlation networks of spinal motor neurons that innervate lower limb muscles during a multi-joint isometric task. *J Physiol* **601,** 3201-3219.

Hug F, Del Vecchio A, Avrillon S, Farina D & Tucker K. (2021b). Muscles from the same muscle group do not necessarily share common drive: evidence from the human triceps surae. *J Appl Physiol (1985)* **130,** 342-354.

Keen DA & Fuglevand AJ. (2004). Common input to motor neurons innervating the same and different compartments of the human extensor digitorum muscle. *J Neurophysiol* **91,** 57-62.

Kennedy PM & Cresswell AG. (2001). The effect of muscle length on motor-unit recruitment during isometric plantar flexion in humans. *Exp Brain Res* **137,** 58-64.

Lacourpaille L, Nordez A & Hug F. (2017). The nervous system does not compensate for an acute change in the balance of passive force between synergist muscles. *J Exp Biol* **220,** 3455-3463.

Laine CM, Martinez-Valdes E, Falla D, Mayer F & Farina D. (2015). Motor Neuron Pools of Synergistic Thigh Muscles Share Most of Their Synaptic Input. *J Neurosci* **35,** 12207-12216.

Laine CM, Yavuz SU & Farina D. (2014). Task-related changes in sensorimotor integration influence the common synaptic input to motor neurones. *Acta Physiol (Oxf)* **211,** 229-239.

Lee SS & Piazza SJ. (2008). Inversion-eversion moment arms of gastrocnemius and tibialis anterior measured in vivo. *J Biomech* **41,** 3366-3370.

Lemon RN. (2008). Descending pathways in motor control. *Annual review of neuroscience* **31,** 195-218.

Levine AJ, Hinckley CA, Hilde KL, Driscoll SP, Poon TH, Montgomery JM & Pfaff SL. (2014). Identification of a cellular node for motor control pathways. *Nat Neurosci* **17,** 586-593.

Loeb GE, Brown IE & Cheng EJ. (1999). A hierarchical foundation for models of sensorimotor control. *Exp Brain Res* **126,** 1-18.

Madarshahian S, Letizi J & Latash ML. (2021). Synergic control of a single muscle: The example of flexor digitorum superficialis. *J Physiol* **599,** 1261-1279.

Marshall NJ, Glaser JI, Trautmann EM, Amematsro EA, Perkins SM, Shadlen MN, Abbott LF, Cunningham JP & Churchland MM. (2022). Flexible neural control of motor units. *Nat Neurosci* **25,** 1492-1504.

Martinez-Valdes E, Negro F, Laine CM, Falla D, Mayer F & Farina D. (2017). Tracking motor units longitudinally across experimental sessions with high-density surface electromyography. *J Physiol* **595,** 1479-1496.

Mazzo MR, Holobar A & Enoka RM. (2022). Association between effective neural drive to the triceps surae and fluctuations in plantar-flexion torque during submaximal isometric contractions. *Exp Physiol* **107,** 489-507.

McIsaac TL & Fuglevand AJ. (2007). Motor-unit synchrony within and across compartments of the human flexor digitorum superficialis. *J Neurophysiol* **97,** 550-556.

Muceli S, Poppendieck W, Holobar A, Gandevia S, Liebetanz D & Farina D. (2022). Blind identification of the spinal cord output in humans with high-density electrode arrays implanted in muscles. *Science advances* **8,** eabo5040.

Negro F & Farina D. (2012). Factors influencing the estimates of correlation between motor unit activities in humans. *PLoS One* **7,** e44894.

Negro F, Holobar A & Farina D. (2009). Fluctuations in isometric muscle force can be described by one linear projection of low-frequency components of motor unit discharge rates. *J Physiol* **587,** 5925-5938.

Negro F, Muceli S, Castronovo AM, Holobar A & Farina D. (2016a). Multi-channel intramuscular and surface EMG decomposition by convolutive blind source separation. *J Neural Eng* **13,** 026027.

Negro F, Yavuz US & Farina D. (2016b). The human motor neuron pools receive a dominant slow-varying common synaptic input. *J Physiol* **594,** 5491-5505.

Oliveira AS & Negro F. (2021). Neural control of matched motor units during muscle shortening and lengthening at increasing velocities. *J Appl Physiol (1985)* **130,** 1798-1813.

Overduin SA, d'Avella A, Carmena JM & Bizzi E. (2012). Microstimulation activates a handful of muscle synergies. *Neuron* **76,** 1071-1077.

Rodriguez-Falces J, Negro F & Farina D. (2017). Correlation between discharge timings of pairs of motor units reveals the presence but not the proportion of common synaptic input to motor neurons. *J Neurophysiol* **117,** 1749-1760.

Ronzano R, Lancelin C, Bhumbra GS, Brownstone RM & Beato M. (2021). Proximal and distal spinal neurons innervating multiple synergist and antagonist motor pools. *Elife* **10**.

Rossato J, Tucker K, Avrillon S, Lacourpaille L, Holobar A & Hug F. (2022). Less common synaptic input between muscles from the same group allows for more flexible coordination strategies during a fatiguing task. *J Neurophysiol* **127,** 421-433.

Segal RL, Wolf SL, DeCamp MJ, Chopp MT & English AW. (1991). Anatomical partitioning of three multiarticular human muscles. *Acta Anat (Basel)* **142,** 261-266.

Takei T, Confais J, Tomatsu S, Oya T & Seki K. (2017). Neural basis for hand muscle synergies in the primate spinal cord. *Proc Natl Acad Sci U S A* **114,** 8643-8648.

Tanzarella S, Muceli S, Santello M & Farina D. (2021). Synergistic Organization of Neural Inputs from Spinal Motor Neurons to Extrinsic and Intrinsic Hand Muscles. *J Neurosci* **41,** 6878-6891.

ter Haar Romeny BM, van der Gon JJ & Gielen CC. (1984). Relation between location of a motor unit in the human biceps brachii and its critical firing levels for different tasks. *Experimental neurology* **85,** 631-650.

Thompson CK, Negro F, Johnson MD, Holmes MR, McPherson LM, Powers RK, Farina D & Heckman CJ. (2018). Robust and accurate decoding of motoneuron behaviour and prediction of the resulting force output. *J Physiol* **596,** 2643-2659.

Ting LH, Chiel HJ, Trumbower RD, Allen JL, McKay JL, Hackney ME & Kesar TM. (2015). Neuromechanical principles underlying movement modularity and their implications for rehabilitation. *Neuron* **86,** 38-54.

Tresch MC & Jarc A. (2009). The case for and against muscle synergies. *Curr Opin Neurobiol* **19,** 601-607.

Tresch MC, Saltiel P & Bizzi E. (1999). The construction of movement by the spinal cord. *Nat Neurosci* **2,** 162-167.

Trypidakis G, Amiridis IG, Enoka R, Tsatsaki I, Kellis E & Negro F. (2022). Ankle Angle but Not Knee Angle Influences Force Fluctuations During Plantar Flexion. *Int J Sports Med* **43,** 131-137.

van den Hoorn W, Hodges PW, van Dieen JH & Hug F. (2015). Effect of acute noxious stimulation to the leg or back on muscle synergies during walking. *J Neurophysiol* **113,** 244-254.

Yaron A, Kowalski D, Yaguchi H, Takei T & Seki K. (2020). Forelimb force direction and magnitude independently controlled by spinal modules in the macaque. *Proc Natl Acad Sci U S A* **117,** 27655-27666.